HHS Public Access

Author manuscript

Neuron. Author manuscript; available in PMC 2020 November 20.

Published in final edited form as:

Neuron. 2019 November 20; 104(4): 711–723.e3. doi:10.1016/j.neuron.2019.08.015.

Visual cortex gains independence from peripheral drive before eye opening

Alexandra Gribizis[1], **Xinxin Ge**[1], **Tanya L. Daigle**[2], **James Ackman**[3], **Hongkui Zeng**[2], **Daeyeol Lee**[1,4], **Michael C. Crair**[1,5]

[1]Department of Neuroscience, Yale University School of Medicine, New Haven, Connecticut 06510, USA

[2]Allen Institute for Brain Science, Seattle, WA 98109, USA.

[3]Department of Molecular, Cell, and Developmental Biology, University of California, Santa Cruz, Santa Cruz, CA 95064, USA.

[4]Present address: The Zanvyl Krieger Mind/Brain Institute, Johns Hopkins University, Baltimore, Maryland 21218, USA

[5]Lead Contact, michael.crair@yale.edu

Summary

Visual spatial perception in the mammalian brain occurs through two parallel pathways: one reaches the primary visual cortex (V1) through the thalamus, another the superior colliculus (SC) via direct projections from the retina. The origin, development, and relative function of these two evolutionarily distinct pathways remain obscure. We examined the early functional development of both pathways by simultaneously imaging pre- and post-synaptic spontaneous neuronal activity. We observed that the quality of retinal activity transfer to the thalamus and superior colliculus does not change across the first two postnatal weeks. However, beginning in the second postnatal week, retinal activity does not drive V1 as strongly as earlier wave activity, suggesting that intrinsic cortical activity competes with signals from the sensory periphery as the cortex matures. Together, these findings bring new insight into the function of the SC and V1 and the role of peripheral activity in driving both circuits across development.

AUTHOR CONTRIBUTIONS

Conceptualization, A.G. and M.C.C.; Methodology, A.G., J.B.A., D.L., M.C.C.; Software, A.G. and X.G.; Formal Analysis, A.G. and M.C.C., Investigation, A.G.; Resources, T.D., H.Z., and M.C.C.; Writing-Original Draft, A.G. and M.C.C.; Writing-Review & Editing, A.G., X.G., J.B.A., D.L., and M.C.C.; Visualization, A.G. and M.C.C; Funding Acquisition, A.G. and M.C.C.

DECLARATION OF INTERESTS

The authors declare no competing interests.

Data and Code Availability

Calcium signal detection and analysis was performed using custom MATLAB routines that can be found at: github.com/agribizis/CrairLabCode.

The datasets generated during and/or analyzed during the current study and all custom scripts and functions generated or used during the current study are available from the Lead Contact (michael.crair@yale.edu) on request.

eTOC blurb:

By simultaneously measuring input activity and output activity, Gribizis et al. show that peripheral spontaneous retinal activity consistently and strongly drives response in the midbrain superior colliculus during development, while the cortex becomes progressively *less* sensitive to peripheral drive.

Keywords

retinal waves; spontaneous activity; RCaMP; jRCaMP1b; activity-dependent development; retinal ganglion cells; activity transfer; visual system development; visual cortex; retina; lateral geniculate nucleus; superior colliculus

Introduction

The nervous system is organized to allow for efficient and stable processing of information from the peripheral senses into the rest of the central nervous system. Through the evolutionary expansion of the forebrain, visual scene analysis increasingly migrated from the midbrain (superior colliculus or optic tectum in non-mammals) to the occipital cortex (Zhaoping, 2016). Both the SC and V1 are higher-order feature processing centers with a comprehensive representation of the visual world. One (SC) is thought to be generally more primitive in its visual processing capabilities, the other (V1) evolutionarily newer and more proficient. The development of each of these feature processing centers and how they change in their response to retinal afferent activity is not fully understood, but could help shed light on the computational principles and their respective functional roles in visual processing.

Before the onset of sensory experience, many developing circuits spontaneously generate neural activity. In the neonatal retina, before the retina responds to light, spontaneous activity is generated in the form of traveling waves (Blankenship and Feller, 2010), which are responsible for the refinement of connectivity between the retina and its downstream targets (Burbridge et al., 2014; Kirkby et al., 2013). During the first week after birth in rodents, these waves propagate through the ascending visual pathway from the retina to the SC and thalamus, eventually reaching the visual cortex (Ackman et al., 2012; Colonnese and Khazipov, 2010; Siegel et al., 2012). The reliability of wave propagation into higher order brain centers is unknown, and its extent beyond the first postnatal week has not been characterized.

Three separate epochs of developmental waves have been described in the mammalian visual system, each with unique cellular and pharmacological signatures (Table 1). Retinal waves are first mediated by gap junctions (stage 1: late gestation in rodents) and then depend on cholinergic synaptic transmission (stage 2: from birth until P9–10 in mouse) (Akrouh and Kerschensteiner, 2013; Blankenship and Feller, 2010; Huberman et al., 2008; Kirkby et al., 2013). Stage 2 waves propagate with random trajectories over large areas, but become slower, smaller, and denser as $GABA_A$ signaling matures after postnatal day (P)7 (Maccione et al., 2014). Finally, glutamate signaling between bipolar cells takes over as the main driver of RGCs at around P10 in mouse, causing profound changes in activity dynamics, including

more repetitive trajectories (stage 3: P10–12; Maccione et al., 2014). During stage 2 waves, RGCs transmit signals from the eye to the superior colliculus (SC), lateral geniculate nucleus (dLGN), and up to the primary visual cortex (V1) (Ackman et al., 2012). This process is crucial for the formation of visual system circuitry, including retinotopic map refinement and eye-specific segregation within the dLGN and SC (Ackman et al., 2012; Burbridge et al., 2014). Disrupting stage 2 retinal waves causes a decoupling of activity in retinorecipient regions, the SC and dLGN, from their presynaptic RGC partners (Burbridge et al., 2014).

During glutamatergic (stage 3) waves, neighboring RGCs with opposite light responses (ON-vs. OFF-responsive) are recruited sequentially (Kerschensteiner et al., 2008; Akrouh and Kerschensteiner, 2013), a process regulated by amacrine cells coordinating a crossover inhibitory circuit in the retina that allows ON bipolar cells to control glutamate release from OFF bipolar cells (Akrouh and Kerschensteiner, 2013; Firl et al., 2015). Previous work has highlighted key differences between stage 2 retinal waves measured *in vitro* and *in vivo*, including preferential wave-initiation sites and spatiotemporal wave correlations between the two hemispheres (Ackman et al., 2012; Burbridge et al., 2014). These findings, coupled with inconsistencies in stage 3 wave measurements *in vitro* (Akrouh and Kerschensteiner, 2013; Blankenship et al., 2009; Firl et al., 2015; Maccione et al., 2014), suggest the need for an *in vivo* examination and comparison of stage 3 waves to stage 2.

Early spontaneous activity in primary visual cortex may play a role in the maturation of receptive fields (RFs) and visual function. Orientation maps found in higher mammals, consisting of columns of cells tuned to stimuli of similar orientations, develop without vision (Chapman et al., 1996; Crair et al., 1998; White et al., 2001), but to varying degrees of maturity and reliability (Buisseret and Imbert, 1976; Chapman et al., 1996; Sherk and Stryker, 1976; Smith et al., 2015; Weliky and Katz, 1997; White et al., 2001). In the mouse visual cortex, orientation and direction selective neurons are also present at eye-opening, possibly reflecting the greater abundance of direction selective RGCs and/or more highly tuned thalamic RFs, but their selectivity improves with vision (Hoy and Niell, 2015; Rochefort et al., 2011). While spontaneous activity before eye opening is important for the development of visual response features in visual cortex, the degree to which spontaneous retinal waves influence ongoing activity in visual cortex during and across development is poorly understood.

To understand sensory encoding in the brain, we must first understand how signals are transferred between the sensory periphery and downstream brain regions. Recording activity from two synaptically connected populations of cells, required to measure the strength of peripheral drive on CNS response, has previously been a slow and low yield process (Bruno and Sakmann, 2006; Sedigh-Sarvestani et al., 2017). With new widefield calcium imaging techniques, a better understanding of sensory encoding across entire brain regions is attainable, however measuring activity simultaneously from both afferents and target cells was not previously feasible given their spatial overlap. In the current study, we overcame these limitations by developing a method to measure presynaptic and postsynaptic neurons simultaneously using a red-shifted calcium indicator in one cell population, and green in the other. Thus, with the strategic use of spontaneous activity as peripheral drive and

simultaneous imaging with two fluorophores, we examine how visual activity transfers to downstream targets over the course of development.

We focus on the influence of early spontaneous retinal activity on the visual thalamus, superior colliculus and cortex. We demonstrate specifically that early in development both the SC and V1 are relatively quiescent and attentive to retinal influence. However, around the time of eye opening, the cortex develops an independent pattern of activity that makes it less faithful to thalamic inputs and peripheral drive, while the colliculus continues to faithfully track retinal activity. These experiments significantly extend our understanding of retinal waves and how peripheral spontaneous activity drives cortical and midbrain activity *in vivo* (Ackman et al., 2010; Burbridge et al., 2014), and suggest a fundamental difference in the way the midbrain and cortex process sensory information.

Results

Simultaneously recording pre- and post-synaptic activity using jRCaMP1b and GCaMP6f

Early spontaneous activity percolates into downstream visual areas, but the extent to which each downstream visual area responds to retinal activity across development is unknown. To answer this question, we developed an approach to label retinal ganglion cells and SC neurons with different fluorophores and separately but simultaneously image the activity of these two different cell populations (Fig. 1A–B). We labeled RGC axons with a recently developed red-shifted calcium indicator (jRCaMP1b, see (Dana et al., 2016)), and neurons in the SC with GCaMP6f. Selective labeling of RGC axons with RCaMP was achieved with viral delivery to the retina, and specific labeling of GCaMP6 in the midbrain was accomplished through conditional expression (En1-Cre x floxed GCaMP6, Burbridge et al., 2014). We separately measured the activity of retinal and SC neurons by alternating presentation of 575nm (RCaMP) and 475nm (GCaMP) wavelength excitation light and splitting the emission light into two pathways with different filters to separate the RCaMP and GCaMP fluorescence (See STAR Methods for more detail). In control mice with jRCaMP1b in retinal axons but no GCaMP expression, RCaMP emission was undetectable with GCaMP (475 nm) excitation (Fig. 1C and 1F). In control mice with GCaMP6 expression but no RCaMP, the long tail of GCaMP emission (Akerboom et al., 2013) resulted in weak signals when stimulated with 575nm light and viewed through the GCaMP-specific emission filter (Fig. 1D **top left panel** and 1G), but no signal through the RCaMP-specific emission filter (Fig. 1D **bottom left panel** and 1G). Imaging both RCaMP and GCaMP simultaneously yielded robust and specific signals through the RCaMP and GCaMP exclusive emission filters (Fig. 1E and 1H), which was confirmed by the absence of RCaMP signal in the Inferior Colliculus (IC, Babola et al., 2018) (Fig. 1E **bottom left panel**) when there is robust GCaMP signal in the SC and IC (Fig. 1E **top right panel**), demonstrating that we can simultaneously and separately image activity in two overlapping neural populations in the same field of view.

Activity transfer from retina to downstream targets

With this approach, we imaged RGC axons and SC neurons in the superior colliculus and recorded stage 2 and stage 3 retinal waves to examine the capability of the retina to drive

postsynaptic SC neuron activity (Figure 2, Movie S1). To begin with, we imaged RGC and SC activity in nAChR knockout mice (KO), so called 'waveless mice' (Bansal et al., 2000; Burbridge et al., 2014). These mice were previously reported to have distinctly disrupted spontaneous retinal waves, and activity in SC neurons that is often quite different from that found in the retina (Burbridge et al., 2014). When simultaneously imaging RGC and SC neuron activity in nAChR KO mice, we observed a clear mismatch, with frequent postsynaptic activity that lacked corresponding presynaptic activity (Fig. 2A–D). In contrast, in wild type mice activity in the SC closely tracked RGC activity during both stage 2 and stage 3 waves (Fig. 2A–D). This is reflected in the weak pre- to post-synaptic correlation in nAChR KO mice relative to wild type mice (Fig. 2C), and the frequent independent postsynaptic activity in nAChR KO mice relative to wild type mice (Fig. 2D). There was no difference in either of these measures between stage 2 and stage 3 waves in wild type mice (Fig. 2C, D).

Our simultaneous RGC and SC neuron imaging experiments allowed us to characterize whether and how the nature of synaptic integration changed across development. More specifically, to quantify the relative effects of retinal vs. intra-collicular activity on the postsynaptic activity in a given location, we applied a multiple linear regression approach in which the predicted postsynaptic activity was given by a 2D convolution of retinal and collicular activity (Fig. 2E and see Fig. S1 and STAR Methods). As expected, model predictions of postsynaptic activity were quite good in wild type mice (both stage 2 and stage 3), but weak in nAChR KO mice (Fig. 2Eii), reflecting the independent activity of SC neurons and RGC axons in these mice (Burbridge et al., 2014; Dhande et al., 2011). An analysis of the weighted variance of the presynaptic (β_1) coefficients (see STAR Methods for more details) demonstrates that the influence of RGC axon activity on SC neurons is wide spread in nAChR KO mice, but more focal and similar in spread in stage 2 and stage 3 wild type mice (Fig. 2Eiii, 79.1 ± 15.4μm diameter for stage 2, n = 9, and 81.4 ± 6.8μm stage 3 WT, n = 8, 95.6 μm ± 6.5μm for nAChR KO, n = 8). This is consistent with the anatomical spread of RGC axons in wild type mice (~100μm), which complete their retinotopic refinement by the end of the first week, and the significantly larger spread of retinocollicular arbors in nAChR KO mice (~150μm) (Burbridge et al., 2014; Dhande et al., 2011). The total strength of the contribution of RGC axons on SC neuron activity, measured as the integrated amplitude of the presynaptic (β_1) coefficients, did not differ between nAChR KO, stage 2 or stage 3 wild type mice (Fig. 2Eiv). Overall, these results indicate that the spatial spread and strength of the transfer of RGC activity to SC neurons does not differ significantly between stage 2 and stage 3 wild type mice, but the influence of the retina on SC neuron activity was significantly wider spread in nAChR KO mice.

Stage 3 retinal waves are very different from stage 2 *in vivo*.

Given that the transfer between the retina and SC did not change during the first two postnatal weeks, we next wanted to assess whether stage 3 waves were different from stage 2, which has not previously been measured *in vivo*. To examine late-stage (P10-P12 or 'stage 3') spontaneous retinal waves *in vivo*, we imaged RGC axon terminal activity in the SC using widefield imaging, as previously described for stage 2 waves (Ackman et al., 2012). (Figure 3A–B, Movies S2 and S3, see STAR Methods for further detail.) Retinal

axon terminals were imaged specifically through the conditional expression of GCaMP6f in retinal ganglion cells (Rx-Cre X Ai95). Late stage (stage 3) waves were much more frequent (Figure 3C–D) and faster in their movement trajectory than earlier stage 2 (P5-P8) waves, but traveled a similar distance across the retinal field (Figure S2). Unlike stage 2 waves, which have large and continuous wave fronts, stage 3 waves typically broke up into wavelets with small areas (Fig. 3E). The duration of stage 3 waves was also significantly shorter, both in the overall wave duration across the retina and in the duration of activity in a given location (pixel-based duration, Fig. 3F and Figure S2). Finally, late-stage waves were much more directional in their trajectory of propagation across the retina than was observed at earlier ages (Fig. 3G).

Over the course of the first two weeks of postnatal development, the cerebral cortex gradually grows over the top of, and partially obscures, the SC. We considered the possibility that the directionality of late-stage waves might be an artifact of this overgrowth at later ages; for example, if waves were moving in a uniformly centrifugal pattern, we would only capture the rostral-to-caudal direction of motion in the most caudal section of the SC that remains unobscured by the cortex. To test this possibility, we examined late-stage wave propagation in the SC of mice with a cortex-specific genetic manipulation that dramatically suppresses cortical development. In these cortex-less mice (Shanks et al., 2016), nearly the entire SC is accessible to imaging throughout the first two postnatal weeks (Figure S3). The data from these mice show that late-stage spontaneous wave activity does, in fact, propagate preferentially in a rostral-to-caudal direction throughout the entire retinotopic map.

To examine the mechanism of wave propagation, we applied pharmacological agents to the retina and imaged the resultant effects on wave propagation in retinal axon terminals in the superior colliculus. Consistent with previous descriptions of retinal wave activity *in vivo* (Ackman et al., 2012), we observed that stage 2 retinal waves were abolished by the nicotinic acetylcholine receptor (nAChR) function blocking agent, epibatidine, but not by a combination of glutamate receptor antagonists, NBQX and APV. In contrast, and consistent with previous *in vitro* reports (Bansal et al., 2000; Firl et al., 2015; Maccione et al., 2014; Wong and Wong, 2001; Zhou and Zhao, 2000), stage 3 (P10-P12) retinal waves were blocked by the glutamate receptor antagonists NBQX and APV, but not by epibatidine (Figure S2). These *in vivo* data are consistent with a model of retinal wave propagation, based on *in vitro* experiments, in which stage 2 wave propagation is mediated by acetylcholine receptor signaling amongst a network of amacrine cells, and stage 3 waves are mediated by glutamate release by bipolar cells (Blankenship and Feller, 2010).

In addition to the primary excitatory drivers of retinal waves (acetylcholine and glutamate), *in vitro* data suggests that inhibition of bipolar cells by amacrine cells modulates stage 3 retinal wave propagation (Akrouh and Kerschensteiner, 2013; Blankenship and Feller, 2010; Huberman et al., 2008; Kirkby et al., 2013). Retinal application of a cocktail of inhibitory antagonists (TPMPA, gabazine, and strychnine) *in vivo*, as previously used *in vitro* (Akrouh and Kerschensteiner, 2013), had a pronounced effect on stage 3 but not stage 2 wave propagation (Fig. 3H). Application of the inhibitory cocktail disrupted many of the properties unique to stage 3, namely the multiple, frequent waves become a single,

infrequent wave front similar to what is observed in stage 2 waves (Fig. 3I–J, Movie S4). The effects of the inhibitory antagonists were dose dependent, and were apparent at a concentration 10X that used *in vitro*, but had no apparent effect at a 5X concentration (Figure S2). These experiments confirm that, despite the consistent transfer of retinal activity to the SC during the first two postnatal weeks, stage 3 waves were quite different from stage 2 waves *in vivo*.

Thalamus influence on cortex decreases from stage 2 to stage 3

We next performed a similar model-based analysis as described above for the retina to SC transfer (Figure 2), but this time between the thalamus and the visual cortex (Figure 4). To achieve this, we used Sert-Cre X Ai162 mice, which express GCaMP in the dLGN but not V1, and expressed jRCaMP1b broadly throughout the cortex using AAV delivery via the sinus (Fig. 4A–4C, Barson, Hamodi et al., 2018 bioRxiv 468348; Hamodi et al., 2019; and also see Methods for more detail). Unlike in the SC, where the transfer from retinal axons to the colliculus does not change significantly between wild type stage 2 and stage 3 (Figure 1), we found that the thalamic contribution to V1 activity decreased across development (Fig. 4Fiv), with a significantly larger integrated amplitude of the presynaptic (β_1) coefficients in stage 2 than in stage 3. The presynaptic (β_1) spread, on the other hand, was not significantly different between stage 2 and stage 3, and was maximally efficient at describing the data even when restricted to a 50μm diameter region (Figure S4, 44.8 ± 6.9μm wide in stage 2, n = 7, and 43.8 ± 4.6μm stage 3, n = 6, , 48.1 ± 5.8μm width inhibitory blocker, n = 6). Of note, the typical anatomical spread of a thalamocortical arbor (~500μm) (Antonini et al., 1999; Lee et al., 2005) is ten times the functional spread observed here (~45μm).

Blocking retinal inhibition transformed stage 3 waves into larger stage-2 like waves and resulted in a higher correlation between thalamic and cortical activity (Fig. 4D). However, the application of inhibitory antagonists to the retina did not affect the functional transfer between the thalamus and cortex (Fig. 4F). We considered the possibility that the size of waves might influence transfer properties, or that an increase in cortico-cortical activity at older ages might contribute to smaller β coefficients during stage 3 waves. To examine this, we reanalyzed only the data from frames with high (zscore >2) thalamic activity or high cortical activity (Figure S4), however this did not significantly affect the regression results. The fit of the model was not significantly different in stage 3 than in stage 2 (Fig. 4Fii), indicating that the decrease in the amplitude of the regression coefficients (integrated amplitude) did not stem from a poor model fit. These data demonstrate that the strength by which the thalamus drives the cortex *decreases* across developmental ages, and is much more focal than the typical anatomical spread of a thalamocortical axon arbor.

Stage 3 wave activity transfers well to dLGN, but not V1

To further examine the relationship of retinal activity to downstream targets, we compared retinal activity to thalamic and cortical activity across development. First, we simultaneously imaged retinal and thalamic activity through the conditional expression of GCaMP6s in thalamic afferents (with Sert-Cre X Ai162 mice) and viral transfection of RGCs with GCaMP6f (Fig. 5A, also see STAR Methods). The spontaneous wave activity observed in thalamic afferents in the visual cortex was similar to retinal afferent activity observed in the

SC (Figure S5, also see Movie S5), where small stage 3-like waves track smoothly across thalamic axons in V1 simultaneously with retinal axons in the SC. The retinotopic map in the primary visual cortex (V1) is rotated and flipped with respect to the map observed in the SC (Fig. 5C). When we take this rotation into consideration, the increased directionality in thalamic waves (Figure S5) during stage 3 matches that previously observed in the retinal axons in the SC (Figure 3).

Next, we simultaneously imaged retinal afferent activity in the SC and cortical activity in V1 using Rx-Cre X Ai95 mice, which express GCaMP6 in both retinal afferents and cortex, but not the SC or thalamus (Fig. 5B). Using the previously described method of turning stage 3 waves into waves with stage 2-like properties via the application of inhibitory antagonists to the retina (Fig. 3), as expected we observed larger stage 2-like waves in the cortex of older animals when applying inhibitory antagonists to the retina (Fig. 5B, Figure S5). We used seed-based correlations to measure the strength of the correspondence between retinal waves and thalamic waves, or retinal waves and cortical waves. The strength of seed-based correlations between RGC activity and dLGN activity was not significantly different in stage 3 compared to stage 2 (Fig. 5D–5E). Similarly, the strength of seed-based correlations was not significantly different between RGCs and dLGN or RGCs and V1 during stage 2, but retinal activity during stage 3 was significantly less correlated to the cortex than to the thalamus during stage 2 (Fig. 5E). The seed-based correlation of stage 3 retinal activity with the cortex was not significantly different than stage 2 ($p=0.06$ after correcting for multiple comparisons). We used a second, more robust measure of correspondence between retinal activity and thalamic or cortical activity by calculating the full-field correlation, instead of a local seed-based correlation (Fig. 5F). This measure revealed that the retina was significantly less correlated to V1 during stage 3 than stage 2 or the thalamus in either stage 2 or stage 3 (Fig. 5F). Converting stage 3 waves to stage 2-like waves through the application of inhibitory antagonists to the retina significantly increased the full-field correlation between RGCs and V1 such that it was indistinguishable from stage 2 correlations in the cortex or between RGCs and the dLGN (Fig. 5E, F). Overall, this data indicates that spontaneous RGC activity translated with reasonably high fidelity to the dLGN during both the first and second week (stage 2 and stage 3), but the transfer of RGC activity to V1 was much stronger in the first week (stage 2) than the second week (stage 3).

Discussion

Retinal waves play an important role in the development of the visual system (Cang and Feldheim, 2013; Huberman et al., 2008; Seabrook et al., 2017). Previous work measured the properties of early stage 2 cholinergic retinal waves *in vivo* (Ackman et al., 2012; Burbridge et al., 2014). Here, we extended those observations to provide a comprehensive description of late-stage retinal waves and how they differ from earlier ages *in vivo*. We also described the features of spontaneous activity in downstream visual targets, including the superior colliculus (SC), thalamus (dLGN) and visual cortex (V1), during the second week after birth, just prior to eye opening. Using a novel approach for simultaneous imaging of pre-synaptic and post-synaptic neural activity with distinct genetically encoded fluorophores, which will be useful for a wide variety of future studies, we further examined the fidelity of retinal wave transmission to downstream visual areas. Our observations demonstrate that the

transfer of retinal activity to the SC and dLGN remains faithful across development, but late-stage retinal waves are much less capable of driving the visual cortex than early spontaneous activity. This suggests that the emergence of underlying cortical activity may mask or override signals from the sensory periphery as the cortex matures. These experiments reveal distinct developmental and functional features of the superior colliculus and visual cortex that emphasize the reflexive role of the midbrain and the more complex cognitive role of the cortex in visual scene processing.

Simultaneous imaging between synaptically linked neural populations

A dramatic advantage of *in vivo* imaging is the ability to investigate the effect of the developing periphery on downstream sensory areas. Previous work (Ackman et al., 2012) showed that retinal waves propagate up to visual cortex at early ages (stage 2 waves). However, little was known about the efficiency or persistence of the transfer of peripheral spontaneous activity to the SC, LGN and V1 across development. To address these issues, we developed an imaging approach that permits simultaneous recording of presynaptic afferents with virally expressed RCaMP and their postsynaptic targets using transgenically expressed GCaMP. This novel approach utilizes separate emission filters for each fluorophore and alternating excitation to cleanly separate the epifluorescence signal from the two cell populations. We observed no difference in the fidelity of retinal activity transfer to the SC between stage 2 (week 1) and stage 3 (week 2), despite striking differences in the spatiotemporal characteristics of these waves. We also used the dual-wavelength imaging approach to confirm previous reports (Burbridge et al., 2014) that the SC acts independently of the retina when retinal activity is reduced to sparse firing in nAChR knockout mice. Further studies will be needed to elucidate the source of independent firing within the SC in nAChR KO mice and other mice devoid of retinal activity, and to test whether such activity may emerge precociously in the thalamus and V1 in the absence of retinal drive.

Developmental changes in functional connectivity

We used a regression model to characterize how the activity in one afferent neural population is conveyed to another. This is analogous to previous efforts that measured receptive fields by finding the optimal weights that map between stimulus and response in early visual and auditory areas (Nishimoto and Gallant, 2011; Nishimoto et al., 2006; Theunissen et al., 2000). The regression model provides an unbiased description of the influence of presynaptic activity on postsynaptic activity without thresholds imposed upon the data or assumptions about what constitutes sufficient wave activity. Moreover, simple correlation measures for the transfer between input and output are confounded by the impact of the spatial pattern of the input activity, while the regression model makes no assumptions about the spatial structure of the activity influence. For example, spatially extended waves in the input population would lead to a broad peak in cross-correlation even if the connectivity between the input and output is spatially restricted. This confound is avoided in a regression analysis. Indeed, we observed that the correlation between presynaptic and postsynaptic neurons increased after application of an inhibitory blocker, while the regression model showed that the amplitude and spread of the presynaptic contribution to postsynaptic activity did not change (Figure 4). This confirms the power and suitability of the regression model for characterizing how the activity in one population of neurons influences another.

Changes in the amplitude and the spread of the retinocollicular and thalamocortical transfer with age provide useful insights into the functional development of these circuits, revealing significant differences between how the thalamus influences the cortex relative to how the retina influences the colliculus across development. However, we avoid direct comparisons of the amplitude of the transfer function between brain regions (e.g. between retinocollicular and thalamocortical) for several reasons. First, the fluorophores used in both conditions were not the same (retinal jRCaMP1b, but thalamic GCaMP6s), significantly impacting relative signal-to-noise for the two presynaptic populations. Second, geometric and tissue properties are very different in the cortex and the colliculus, which impacts the relationship between spatial structure and amplitude. For example, presynaptic thalamic activity was measured through a thicker layer of cortical tissue than the presynaptic retinal activity in the SC, influencing signal to noise and spatial scatter of the presynaptic activity. However, differences in these effects are minimal when comparing thalamocortical or retinocollicular transfer across a short developmental window between stage 2 and stage 3.

Stage 2 vs. stage 3 waves

Stage 3 waves (just before eye opening) are dramatically different from stage 2 waves. *In vitro* studies have previously described the smaller size of stage 3 waves (Elstrott and Feller, 2010; Maccione et al., 2014), which we confirmed *in vivo* in this study. *In vitro* studies have offered conflicting accounts on the biased directionality of wave propagation (Maccione et al., 2014; Stafford et al., 2009), which we observed *in vivo* for stage 3 and to a lesser extent stage 2 waves (Ackman et al., 2012). Overall, many wave properties are similar *in vivo* and *in vitro*, and dissimilarities, such as duration and distance traveled, likely stem from differences in how waves are defined using retinal multi-electrode array recordings *in vitro* vs. calcium imaging *in vivo*.

A unique feature of glutamatergic waves is the asynchronous recruitment of ON and OFF ganglion cells mediated by amacrine cell inhibition (Akrouh and Kerschensteiner, 2013; Kerschensteiner and Wong, 2008). Interestingly, previous *in vitro* studies (Akrouh and Kerschensteiner, 2013; Blankenship et al., 2009; Firl et al., 2015; Kerschensteiner and Wong, 2008) did not reveal the extent to which blocking inhibition significantly changes the quality of stage 3 waves, particularly the conversion from many small wavelets to fewer, infrequent, and larger single wave fronts observed *in vivo*. We believe that the single large wave fronts following inhibitory blockade in the retina are a result of simultaneous firing of ON- and OFF-RGCs. This suggests that inhibition in the retina not only causes asynchronous ON and OFF RGC firing, but also breaks up stage 3 waves into disjoint, small, propagating domains. Unfortunately, current methods do not allow for separately recording groups of ON and OFF RGCs *in vivo*, but we anticipate directly testing this hypothesis in future studies.

Unlike in previously described *in vitro* work (Leitch et al., 2005; Stellwagen et al., 1999), inhibitory antagonists applied to the retina did not block spontaneous activity or waves *in vivo* in the present study. This does not directly contradict the notion that GABA receptors in retinal ganglion cells are depolarizing early in development, but we found no evidence to support this claim *in vivo*.

The development of cortical and subcortical areas

Multielectrode array recordings from the thalamus of the ferret are consistent with our observation of cortical activity that is independent of the retina emerging over development (Weliky and Katz, 1999). Experiments employing simultaneous microelectrode measurements of both thalamus and cortex in the rat provided additional insight into changes in thalamic and cortical activity across development (Murata and Colonnese, 2016). This analysis suggested that a strong thalamocortical excitatory loop is present in the first post-natal week, but not in the second (Murata and Colonnese, 2016). However, the analysis was confined to an examination of temporal correlations between thalamus and cortex because the measurements contained no spatial information. The widefield calcium imaging approach employed here provides both spatial and temporal information about the influence of thalamus on cortex, revealing that thalamic wave activity is less predictive of cortical activity in second-week mice than during the first week. Our data are consistent with earlier experiments, with a stronger thalamocortical transfer function in the first week than the second week, but our data further suggest that cortex-intrinsic activity is not responsible for the changes in thalamic drive we observed.

There are several potential repercussions of this result. Previous computational work suggests that changes in the total conductance of cortical neurons between the first and second postnatal weeks could disrupt the transfer of large wave-like activity (Gjorgjieva et al., 2014). This ‘gain-scaling’ property is absent in developing neurons, which respond to large amplitude events without adaptation, but crucial for information transmission about stimulus fluctuations in the mature brain. Indeed, cortical response to the periphery might necessarily take on a more signal-specific or feature-specific role in the mature cortex, when a heightened response to population activity instead of feature-specific activity may be detrimental rather than computationally informative. Differences between presynaptic influence on postsynaptic activity across development in the thalamocortical system could also be due to changes in corticothalamic feedback. However, several studies demonstrate that significant corticothalamic feedback does not begin until after eye opening (Hooks and Chen, 2006, 2008; Thompson et al., 2016), suggesting that corticothalamic feedback did not contribute to the thalamocortical transfer function or changes with age.

The cortex grows significantly across the first two postnatal weeks of development (stage 3 cortex is 14% larger than stage 2, Figure S4E). We considered whether this expansion may account for the measured change in thalamocortical transfer. If cortical expansion is coupled with an expansion of the thalamic axon projections, then for the thalamocortical transfer function we would expect an increase in presynaptic spread (weighted variance) and a constant presynaptic amplitude (integral), which is the opposite of what we observed (Figure 4F). Another possibility is that thalamic axon projection area remains unchanged, even with an expansion in cortical size. In this case, both the presynaptic spread (weighted variance) and the presynaptic amplitude (integral) should remain unchanged, however this is also not consistent with the data. Instead, what our data show is that while the cortex expands during the first two postnatal weeks, the presynaptic spread (weighted variance) of the thalamocortical transfer remains unchanged, suggesting the point-spread function between the retina and the visual representation in V1 may actually become more focused in light of

the cortical expansion. In addition, the relative weight of the thalamocortical connection diminishes, as shown by the change in the presynaptic amplitude (integral).

Interestingly, we did not see a measurable difference in the amplitude or spatial extent of the transfer between the retina and the colliculus over the same developmental period. Colliculus activity that is independent of the retina may develop later than in the cortex, but this runs counter to the general precociousness of midbrain development relative to the cortex. It is also possible that the cortex but not the colliculus becomes endogenously active in the second postnatal week, which would contribute to the measured decrease in thalamic contribution to cortical activity at older ages. We tested this explanation by running the regression analysis only for times when the cortex and thalamus were simultaneously active – even still the thalamic input was weaker in stage 3 than stage 2 (Figure S4). This suggests that changes in the thalamocortical transformation itself, even at times of high correlation, are a dominant cause of the decrease in thalamocortical drive just before eye opening.

Spatial spread of retinocollicular and thalamocortical influence

The anatomical spread of retinal ganglion cell afferent projections to colliculus is approximately 100μm (Dhande et al., 2011), which is similar to but somewhat larger than the spatial spread of the retinocollicular transfer function (Figure 2, 81.4 ± 6.8μm). In contrast, LGN afferent projections to the cortex are approximately 500μm (Antonini et al., 1999; Lee et al., 2005), which is 10-fold larger than the spatial spread of the thalamocortical transfer function, 43.8 ± 4.6μm (Figure 4, S4). The much more focal nature of the functional transfer of thalamus to visual cortex, compared to either the anatomical spread of thalamocortical arbors or functional spread of retinal influence in the SC, may reflect the preference for local integration in thalamocortical synaptic connections (Scholl et al., 2017). Presumably, cortical cells selectively integrate functional features from different thalamic neurons to construct new receptive field properties, rather than summing input generically from a broad population of retinotopically matched afferents.

Species with a different emphasis on cortical and subcortical processing may integrate thalamocortical activity differently (Zhaoping, 2016). For example, several studies have shown that the organization of orientation preference in mouse V1 is scattered or organized in a ‘salt and pepper’ formation, whereas in the mouse SC, neurons with similar orientation preference cluster together (Feinberg and Meister, 2015). Orientation maps in the visual cortex of other mammals, such as cats, ferrets and primates, are much more spatially structured with both local and long-range order (Chapman et al., 1996; Crair et al., 1998; White et al., 2001). The developing mouse cortex may be organized in local, feature-specific patterns that do not benefit from the integration of thalamic afferents over large areas with inconsistent feature preferences, while the SC is less selective when integrating feature preferences, resulting in a stronger transfer function suitable for its more reflexive role in behavior. We believe the results and approaches demonstrated here will be broadly useful in future studies of visual circuitry and physiology, as well as the examination of the functional relationship between populations of afferents and efferents in neural populations elsewhere in the brain.

STAR Methods

Contact for Reagent and Resource Sharing

Further information and requests for resources and reagents should be directed to and will be fulfilled by the Lead Contact, Michael C. Crair (michael.crair@yale.edu).

Experimental Model and Subject Details

Animals—All mice used in this study were between 5 and 12 days of age and were of both sexes. Animal care and use followed the Yale Institutional Animal Care and Use Committee (IACUC), the US Department of Health and the Human Services, and institution guidelines. Neonatal mice (C57BL/6J) Ai95 floxed GCaMP6, crossed with *Rx-Cre* (Ackman et al., 2012; Swindell et al., 2006) aged 5–12 days after birth (postnatal day 5–12, P5-P12) were used for experiments depicted in figures 3 and 5. En1-Cre X floxed-GCaMP6 (Dhande (Burbridge et al., 2014; Dhande et al., 2012)et al., 2012, Burbridge et al., 2014) as well as the nAChR-KO mice (Burbridge et al., 2014) were used for experiments in figures 1 and 2, and Sert-Cre x Ai162 (Daigle et al., 2018) in figures 4 and 5.

Method Details

Surgical procedure for *in vivo* imaging—Mice aged P5 to P12 were surgically prepared for imaging as previously reported (Ackman et al., 2012). The procedure took roughly 40 minutes and was followed by a 3-hr recovery period in the dark under continuously delivered medical oxygen with isoflurane at 0%. The mouse was surrounded by a cotton ball nest during recovery and imaging.

In Vivo Wide Field Calcium Imaging and Dual Wavelength Imaging Approach.—Calcium imaging was performed *in vivo* using wide-field epifluoresence microscopy with a sCMOS camera (pco.edge, PCO) coupled to a Zeiss AxioZoom V16 microscope with 1X macro objective camera. For dual wavelength imaging, an image splitter (Cairn OptoSplit II LS) was attached before the camera with Semrock FF01–624/40–25, Semrock FF01–593/LP-25, and Semrock FF01–525/45–25 filters to project the emission onto two halves of the camera chip. Epifluorescent illumination was provided by an LED source (X-Cite TURBO XLED), using 450–495nm illumination for GCaMP imaging and 540–600nm for RCaMP excitation through a Fitc/Tritc filter cube (Chroma, 59022), and an exposure of 100 msec. Imaging of activity was performed on unanesthetized, head-fixed mice after a 3-hr recovery from isoflurane anesthesia and the surgical procedure to expose the SC. Each recording consisted of a single, continuously acquired movie for 10 min.

During the recordings, the head was fixed under the microscope objective by steel posts attached to the skull, and the body was loosely surrounded by cotton gauze, such that the animals could move on the heating pad. During the experiment, mouse pups spent the majority of time in a quiet, resting state interrupted by brief motor twitches of limbs or tail. Pharmacological manipulation of in vivo spontaneous activity was achieved by reanesthetizing animals using 2% isoflurane for 5–10 min, exposing the eye, and injecting ~500 nL per eye with a pulled glass micropipette using a Nanoject (Drummond Scientific). After injection, the eyelid was closed and covered in ophthalmic ointment and a brief local

anesthetic, and the animal returned to 0% isoflurane before being allowed to recover at least 20–30 minutes.

Eye Injections and Sinus Injections—Perinatal mice are hypothermically anesthetized for 2–3 minutes before surgery, and kept cold for the brief period during surgical injection. Pulled glass micropipettes (1B150F-4; World Precision Instruments) were loaded with AAV-Syn-GCaMP6f or AAV-Syn-jRCaMP1b and then 1–2uL was pressure injected into each ocular vitreous or transverse sinus at P0-P1. Mice are then placed on a temperature-controlled heat pad after surgery and returned to their mothers upon recovery from anesthesia. After retinal injections, we waited 4–5 days for virus to transfect and fill retinal ganglion cell axons. For acute eye injections, either (1) 0.5–1 μl of 10 μM (±)-epibatidine dihydrochloride hydrate (Sigma no. E1145) dissolved in saline, or (2) a cocktail of 1 mM AP5 (Tocris) and 200 μM NBQX (Tocris), or (3) a cocktail of 500 μM 1,2,5,6-Tetrahydropyridine-4-yl-methylphosphinic acid (TPMPA, Sigma), 50 μM gabazine (Tocris), and 5 uM strychnine (Sigma) was pressure injected using a glass micropette inserted into the vitreous.

Quantification and Statistical Analysis

Calcium signal and wave detection.—Automated image segmentation and calcium event detection was performed using custom routines written in MATLAB. The mean pixel intensity at each pixel location, F0 was subtracted and normalized to each frame, Ft of the movie to form a ΔF/F array: A= (Ft-F0)/F0. Each frame was smoothed with a Gaussian having a standard deviation of 56 μm and a signal intensity thresholded at T, which was set to >2 standard deviations of the signal. Calcium domain signals were automatically segmented as contiguously connected components in space and time from this binarized image. A set of regional measurements were obtained from the largest component in the binary wave mask (‘area’, ‘centroid’, ‘eccentricity’, ‘equivdiameter’, ‘extent’, ‘majoraxislength’, ‘minoraxislength’, ‘orientation’ and ‘solidity’ from function ‘regionprops’, MATLAB Image Processing Toolbox), described in detail previously (Ackman et al., 2014, bioRxiv).

Components located outside the boundaries of the region of interest or having a duration of 1 frame were ignored. The number of contiguous frames (bounding box depth) for each segmented calcium domain was taken to be the domain duration. Wave speeds were determined by finding the set of distances for each wave frame’s centroid relative to the wave-onset centroid and calculating the mean of this set. Wave directions were determined by calculating the vector sum of the iterative directions between wave-front centroids in sequential frames for each wave. Measured wave directions in the right hemisphere were mirrored so that the direction values could be compared directly between hemispheres. Wave frequencies for each recording were calculated as the number of waves divided by the length of time for each recording. Inter-wave intervals for each recording were calculated as the set of time intervals between the onsets of sequential waves in each recording. The active fraction for each wave of each hemisphere was the number of pixels participating in a wave divided by the total number of pixels in that recording.

Seed based correlations—Seed based correlations were measured by taking a random sample of 100 pixels from the superior colliculus and computing the cross correlation of the 100 SC pixels with every pixel in V1. The point in V1 with the largest correlation value was chosen as the corresponding retinotopic region for the correlation analysis. Seed-based maps were checked to ensure that they followed a general retinotopic pattern, those that did not were excluded from further analysis (14 out of 50 V1 maps were excluded across conditions). Poor retinotopic correlation resulting in map exclusion was due to low wave variability and limited data; for example, if only a handful of waves occurred, and these waves were moving in the same direction, then there wasn't a distinct retinotopic correlation map.

Statistical analysis—Data sets were analyzed and plotted using custom routines implemented in MATLAB or in GraphPad Prism. Distribution means were compared using two-sample Student's t-tests unless otherwise noted (Wilcoxon Rank Sum test was used for small, non-normally distributed data sets) or using ANOVA followed by Tukey's HSD post-hoc test when analyzing the effects of multiple grouping factors ($p < 0.05$ set as significance). All graphs report medians with the 95% confidence interval unless otherwise noted. Stars in figures indicate the following: * = $p<0.05$, ** = $p<0.01$, *** = $p<0.001$. Values of n and their designations (mice or hemispheres) are indicated in the figure legends; all data was aligned to left hemisphere coordinates before analysis.

Regression Analysis—To quantitatively analyze and identify any change in the capability of retinal axons to transfer activity patterns to SC target neurons during normal development, we modeled the postsynaptic activity at a given pixel in the superior colliculus as a weighted sum of presynaptic and postsynaptic activity convolved with 2 separate 2-D linear kernels. Both presynaptic and postsynaptic regressors used in this model were the ΔF/F values within an area of 13 X 13 pixels (corresponding to 100μm X 100μm) surrounding each postsynaptic pixel of interest. We included both a set of presynaptic predictors to measure the contribution of presynaptic retinal activity on postsynaptic SC neuron activity, and surrounding postsynaptic predictors, to account for the possible contribution of GCaMP6 light scatter and intra-collicular interactions. The response data is taken from each postsynaptic pixel of interest, of which 6 million data points were randomly sampled across all animals, 1 million per each hemisphere. The resulting β estimates (β_0, β_1 and β_2) are the standardized regression coefficients chosen to minimize the sum of squared errors and represent the change in the mean response of the postsynaptic data per unit increase in the associated predictor variable when all other predictors are held constant. A larger β coefficient thereby indicates a stronger association between that variable and the postsynaptic response, whereas a β coefficient near zero indicates no association between the variables. Diameters of regression coefficients were measured by the width of the bounding box for all positive β coefficients. Weighted variance and integral calculations for the spread and amplitude of the response, respectively were measured as indicated below.

Weighted Variance and Integral Calculations—Analysis of regression models was performed using custom MATLAB routines (github.com/agribizis/CrairLabCode). Positive and contiguous regression coefficients were used to calculate weighted variance and integral

values. The integral was calculated as the sum of all positive and contiguous values; weighted variance was calculated as follows:

$$\frac{\Sigma f_{ij}\left[\left(x_i - \bar{x}\right)^2 + \left(y_j - \bar{y}\right)^2\right]}{\Sigma f_{ij}}$$

where x_i and y_j refer to the horizontal or vertical position, respectively, of the coefficient relative to the center $(\bar{x}, \bar{y})$, and f_{ij} is the value of the regression coefficient at location (i, j).

Lead Contact and Materials Availability—This study did not generate new unique reagents.

Supplementary Material

Refer to Web version on PubMed Central for supplementary material.

Acknowledgements

We would like to thank all members of the Crair lab for their helpful comments on this project. This work was supported by NIH grants EY015788, EY023105, and EY025968, and NIH grants P30 EY000785 and R01 EY015788 to M.C.C. and F31EY025968 to A.G. M.C.C. also thanks the family of William Ziegler III for their support.

References

Ackman JB, Burbridge TJ, and Crair MC. (2012). Retinal waves coordinate patterned activity throughout the developing visual system. Nature 490, 219–225. [PubMed: 23060192]

Akerboom J, Carreras Calderon N, Tian L, Wabnig S, Prigge M, Tolo J, Gordus A, Orger MB, Severi KE, Macklin JJ, et al. (2013). Genetically encoded calcium indicators for multi-color neural activity imaging and combination with optogenetics. Front Mol Neurosci 6, 2. [PubMed: 23459413]

Akrouh A, and Kerschensteiner D. (2013). Intersecting circuits generate precisely patterned retinal waves. Neuron 79, 322–334. [PubMed: 23830830]

Antonini A, Fagiolini M, and Stryker MP. (1999). Anatomical correlates of functional plasticity in mouse visual cortex. J Neurosci 19, 4388–4406. [PubMed: 10341241]

Babola TA, Li S, Gribizis A, Lee BJ, Issa JB, Wang HC, Crair MC, and Bergles DE. (2018). Homeostatic Control of Spontaneous Activity in the Developing Auditory System. Neuron 99, 511–524 e515. [PubMed: 30077356]

Bansal A, Singer JH, Hwang BJ, Xu W, Beaudet A, and Feller MB. (2000). Mice lacking specific nicotinic acetylcholine receptor subunits exhibit dramatically altered spontaneous activity patterns and reveal a limited role for retinal waves in forming ON and OFF circuits in the inner retina. J Neurosci 20, 7672–7681. [PubMed: 11027228]

Blankenship AG, and Feller MB. (2010). Mechanisms underlying spontaneous patterned activity in developing neural circuits. Nat Rev Neurosci 11, 18–29. [PubMed: 19953103]

Blankenship AG, Ford KJ, Johnson J, Seal RP, Edwards RH, Copenhagen DR, and Feller MB. (2009). Synaptic and extrasynaptic factors governing glutamatergic retinal waves. Neuron 62, 230–241. [PubMed: 19409268]

Bruno RM, and Sakmann B. (2006). Cortex is driven by weak but synchronously active thalamocortical synapses. Science 312, 1622–1627. [PubMed: 16778049]

Buisseret P, and Imbert M. (1976). Visual cortical cells: their developmental properties in normal and dark reared kittens. J Physiol 255, 511–525. [PubMed: 1255531]

Burbridge TJ, Xu HP, Ackman JB, Ge X, Zhang Y, Ye MJ, Zhou ZJ, Xu J, Contractor A, and Crair MC. (2014). Visual circuit development requires patterned activity mediated by retinal acetylcholine receptors. Neuron 84, 1049–1064. [PubMed: 25466916]

Cang J, and Feldheim DA. (2013). Developmental mechanisms of topographic map formation and alignment. Annu Rev Neurosci 36, 51–77. [PubMed: 23642132]

Chapman B, Stryker MP, and Bonhoeffer T. (1996). Development of orientation preference maps in ferret primary visual cortex. J Neurosci 16, 6443–6453. [PubMed: 8815923]

Colonnese MT, and Khazipov R. (2010). "Slow activity transients" in infant rat visual cortex: a spreading synchronous oscillation patterned by retinal waves. J Neurosci 30, 4325–4337. [PubMed: 20335468]

Crair MC, Gillespie DC, and Stryker MP. (1998). The role of visual experience in the development of columns in cat visual cortex. Science 279, 566–570. [PubMed: 9438851]

Daigle TL, Madisen L, Hage TA, Valley MT, Knoblich U, Larsen RS, Takeno MM, Huang L, Gu H, Larsen R, et al. (2018). A Suite of Transgenic Driver and Reporter Mouse Lines with Enhanced Brain-Cell-Type Targeting and Functionality. Cell 174, 465–480 e422. [PubMed: 30007418]

Dana H, Mohar B, Sun Y, Narayan S, Gordus A, Hasseman JP, Tsegaye G, Holt GT, Hu A, Walpita D, et al. (2016). Sensitive red protein calcium indicators for imaging neural activity. Elife 5.

Dhande OS, Bhatt S, Anishchenko A, Elstrott J, Iwasato T, Swindell EC, Xu HP, Jamrich M, Itohara S, Feller MB, and Crair MC. (2012). Role of adenylate cyclase 1 in retinofugal map development. J Comp Neurol 520, 1562–1583. [PubMed: 22102330]

Dhande OS, Hua EW, Guh E, Yeh J, Bhatt S, Zhang Y, Ruthazer ES, Feller MB, and Crair MC. (2011). Development of single retinofugal axon arbors in normal and beta2 knock-out mice. J Neurosci 31, 3384–3399. [PubMed: 21368050]

Elstrott J, and Feller MB. (2010). Direction-selective ganglion cells show symmetric participation in retinal waves during development. J Neurosci 30, 11197–11201. [PubMed: 20720127]

Feinberg EH, and Meister M. (2015). Orientation columns in the mouse superior colliculus. Nature 519, 229–232. [PubMed: 25517100]

Firl A, Ke JB, Zhang L, Fuerst PG, Singer JH, and Feller MB. (2015). Elucidating the role of AII amacrine cells in glutamatergic retinal waves. J Neurosci 35, 1675–1686. [PubMed: 25632142]

Gjorgjieva J, Mease RA, Moody WJ, and Fairhall AL. (2014). Intrinsic neuronal properties switch the mode of information transmission in networks. PLoS Comput Biol 10, e1003962. [PubMed: 25474701]

Hamodi AS, Sabino AM, Fitzgerald ND, and Crair MC. (2019). Transverse sinus injections: A novel method for whole-brain vector-driven gene delivery. bioRxiv, 579730.

Hooks BM, and Chen C. (2006). Distinct roles for spontaneous and visual activity in remodeling of the retinogeniculate synapse. Neuron 52, 281–291. [PubMed: 17046691]

Hooks BM, and Chen C. (2008). Vision triggers an experience-dependent sensitive period at the retinogeniculate synapse. J Neurosci 28, 4807–4817. [PubMed: 18448657]

Hoy JL, and Niell CM. (2015). Layer-specific refinement of visual cortex function after eye opening in the awake mouse. J Neurosci 35, 3370–3383. [PubMed: 25716837]

Huberman AD, Feller MB, and Chapman B. (2008). Mechanisms underlying development of visual maps and receptive fields. Annu Rev Neurosci 31, 479–509. [PubMed: 18558864]

Kerschensteiner D, and Wong RO. (2008). A precisely timed asynchronous pattern of ON and OFF retinal ganglion cell activity during propagation of retinal waves. Neuron 58, 851–858. [PubMed: 18579076]

Kirkby LA, Sack GS, Firl A, and Feller MB. (2013). A role for correlated spontaneous activity in the assembly of neural circuits. Neuron 80, 1129–1144. [PubMed: 24314725]

Lee LJ, Iwasato T, Itohara S, and Erzurumlu RS. (2005). Exuberant thalamocortical axon arborization in cortex-specific NMDAR1 knockout mice. J Comp Neurol 485, 280–292. [PubMed: 15803506]

Leitch E, Coaker J, Young C, Mehta V, and Sernagor E. (2005). GABA type-A activity controls its own developmental polarity switch in the maturing retina. J Neurosci 25, 4801–4805. [PubMed: 15888655]

Maccione A, Hennig MH, Gandolfo M, Muthmann O, van Coppenhagen J, Eglen SJ, Berdondini L, and Sernagor E. (2014). Following the ontogeny of retinal waves: pan-retinal recordings of population dynamics in the neonatal mouse. J Physiol 592, 1545–1563. [PubMed: 24366261]

Murata Y, and Colonnese MT. (2016). An excitatory cortical feedback loop gates retinal wave transmission in rodent thalamus. Elife 5.

Nishimoto S, and Gallant JL. (2011). A three-dimensional spatiotemporal receptive field model explains responses of area MT neurons to naturalistic movies. J Neurosci 31, 14551–14564. [PubMed: 21994372]

Nishimoto S, Ishida T, and Ohzawa I. (2006). Receptive field properties of neurons in the early visual cortex revealed by local spectral reverse correlation. J Neurosci 26, 3269–3280. [PubMed: 16554477]

Rochefort NL, Narushima M, Grienberger C, Marandi N, Hill DN, and Konnerth A. (2011). Development of direction selectivity in mouse cortical neurons. Neuron 71, 425–432. [PubMed: 21835340]

Scholl B, Wilson DE, and Fitzpatrick D. (2017). Local Order within Global Disorder: Synaptic Architecture of Visual Space. Neuron 96, 1127–1138 e1124. [PubMed: 29103806]

Seabrook TA, Burbridge TJ, Crair MC, and Huberman AD. (2017). Architecture, Function, and Assembly of the Mouse Visual System. Annu Rev Neurosci 40, 499–538. [PubMed: 28772103]

Sedigh-Sarvestani M, Vigeland L, Fernandez-Lamo I, Taylor MM, Palmer LA, and Contreras D. (2017). Intracellular, In Vivo, Dynamics of Thalamocortical Synapses in Visual Cortex. J Neurosci 37, 5250–5262. [PubMed: 28438969]

Shanks JA, Ito S, Schaevitz L, Yamada J, Chen B, Litke A, and Feldheim DA. (2016). Corticothalamic Axons Are Essential for Retinal Ganglion Cell Axon Targeting to the Mouse Dorsal Lateral Geniculate Nucleus. J Neurosci 36, 5252–5263. [PubMed: 27170123]

Sherk H, and Stryker MP. (1976). Quantitative study of cortical orientation selectivity in visually inexperienced kitten. J Neurophysiol 39, 63–70. [PubMed: 1249604]

Siegel F, Heimel JA, Peters J, and Lohmann C. (2012). Peripheral and central inputs shape network dynamics in the developing visual cortex in vivo. Curr Biol 22, 253–258. [PubMed: 22264606]

Smith GB, Sederberg A, Elyada YM, Van Hooser SD, Kaschube M, and Fitzpatrick D. (2015). The development of cortical circuits for motion discrimination. Nat Neurosci 18, 252–261. [PubMed: 25599224]

Stafford BK, Sher A, Litke AM, and Feldheim DA. (2009). Spatial-temporal patterns of retinal waves underlying activity-dependent refinement of retinofugal projections. Neuron 64, 200–212. [PubMed: 19874788]

Stellwagen D, Shatz CJ, and Feller MB. (1999). Dynamics of retinal waves are controlled by cyclic AMP. Neuron 24, 673–685. [PubMed: 10595518]

Swindell EC, Bailey TJ, Loosli F, Liu C, Amaya-Manzanares F, Mahon KA, Wittbrodt J, and Jamrich M. (2006). Rx-Cre, a tool for inactivation of gene expression in the developing retina. Genesis 44, 361–363. [PubMed: 16850473]

Syed MM, Lee S, Zheng J, and Zhou ZJ. (2004). Stage-dependent dynamics and modulation of spontaneous waves in the developing rabbit retina. J Physiol 560, 533–549. [PubMed: 15308679]

Theunissen FE, Sen K, and Doupe AJ. (2000). Spectral-temporal receptive fields of nonlinear auditory neurons obtained using natural sounds. J Neurosci 20, 2315–2331. [PubMed: 10704507]

Thompson AD, Picard N, Min L, Fagiolini M, and Chen C. (2016). Cortical Feedback Regulates Feedforward Retinogeniculate Refinement. Neuron 91, 1021–1033. [PubMed: 27545712]

Weliky M, and Katz LC. (1997). Disruption of orientation tuning in visual cortex by artificially correlated neuronal activity. Nature 386, 680–685. [PubMed: 9109486]

White LE, Coppola DM, and Fitzpatrick D. (2001). The contribution of sensory experience to the maturation of orientation selectivity in ferret visual cortex. Nature 411, 1049–1052. [PubMed: 11429605]

Wong WT, and Wong RO. (2001). Changing specificity of neurotransmitter regulation of rapid dendritic remodeling during synaptogenesis. Nat Neurosci 4, 351–352. [PubMed: 11276221]

Zhaoping L. (2016). From the optic tectum to the primary visual cortex: migration through evolution of the saliency map for exogenous attentional guidance. Curr Opin Neurobiol 40, 94–102. [PubMed: 27420378]

Zhou ZJ, and Zhao D. (2000). Coordinated transitions in neurotransmitter systems for the initiation and propagation of spontaneous retinal waves. J Neurosci 20, 6570–6577. [PubMed: 10964962]

Highlights:

- Second week (‘stage 3’) retinal waves are very distinct from first week (‘stage 2’)
- Stage 3 waves are especially sensitive to inhibitory blockade
- Retinal influence on the colliculus and thalamus does not change over development
- However, cortex becomes relatively *insensitive* to retinal drive before eye opening

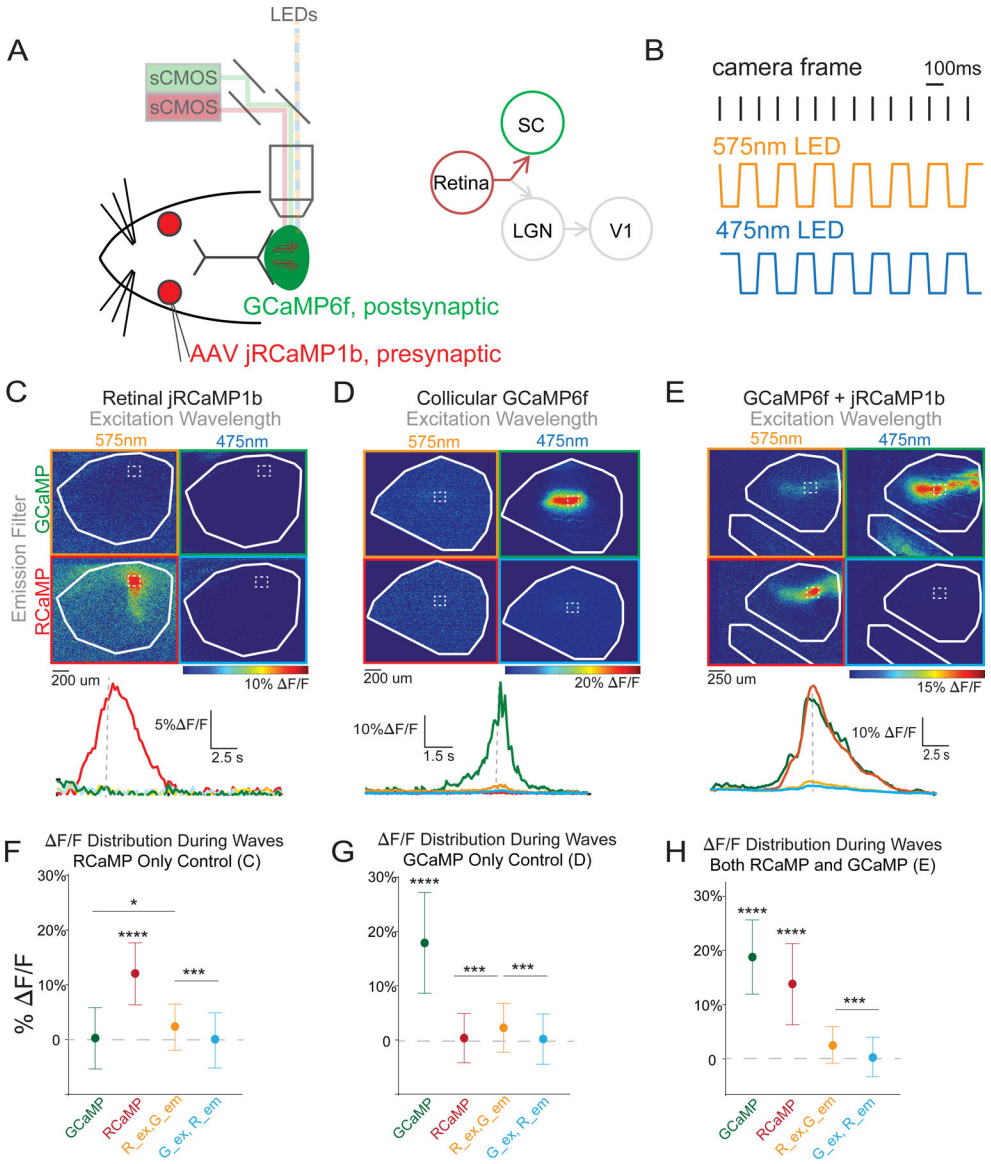

Figure 1: Simultaneously and separately recording pre- and post-synaptic activity using jRCaMP1b and GCaMP6f

(A-B) Experimental setup for dual imaging of GCaMP6f and jRCaMP1b. En1-Cre X Ai95 animals, which express GCaMP6f in the brainstem but not the retina, were injected in the eye with AAV coding for the red-shifted calcium indicator jRCaMP1b. Both pre-synaptic RGC axons and postsynaptic SC neurons were then imaged simultaneously by alternating excitation for jRCaMP1b (475 nm) and GCaMP6f (575 nm) and selective filters for the emission of each fluorophore.

(C) Example control experiment (top) in which jRCaMP1b was expressed in the retina but there was no GCaMP6f. Example illustrates that jRCaMP1b fluorescence (red) did not bleed into the GCaMP6f channel (green). Time course (bottom) of the fluorescence at the position of the dashed square in top panel demonstrates selectivity of the jRCaMP1b fluorescence (red). Dashed grey line (bottom) indicates time of the frame (top).

(D) Same as (C), except GCaMP6f is expressed in the SC but there is no jRCaMP1b. The example illustrates that GCaMP6f fluorescence (green) does not bleed into jRCaMP1b channel (red).

(E) Same as (C-D), but with an experimental animal in which jRCaMP1b is expressed in RGCs and GCaMP6f is expressed in the midbrain colliculus. White arrow shows GCaMP6f spontaneous activity in the inferior colliculus (IC), which served as a further control to check for the exclusion of GCaMP6f emission from the jRCaMP1b channel.

(F) Summary quantification of (C). Fluorescent signal (ΔF/F) during a wave is limited to the jRCaMP1b channel when jRCaMP1b is selectively expressed in RGCs.

(G) Summary quantification of (D). Fluorescent signal (ΔF/F) during a wave is limited to the GCaMP6f channel when GCaMP6f is selectively expressed in SC neurons.

(H) Summary quantification of (E). Fluorescent signal (ΔF/F) during a wave shows simultaneous GCaMP6f and jRCaMP1b signal when jRCaMP1b is expressed in RGCs and GCaMP6f is expressed in SC neurons.

* = $p<0.05$, ** = $p<0.01$, *** = $p<0.001$, t-test.

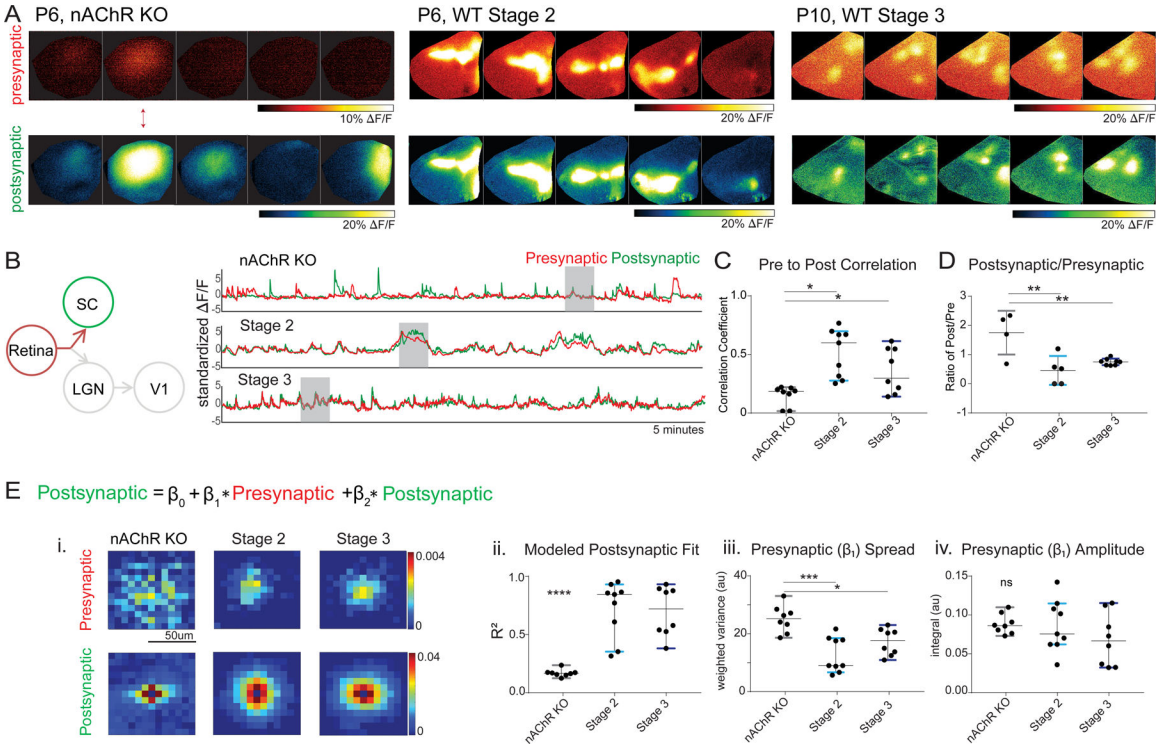

Figure 2. Transfer function of Stage 2 retinal waves to SC is not significantly different from transfer function of Stage 3 retinal waves to SC; SC activity can be predicted from retinal activity

(A) Three montage examples of wave types that were analyzed, nAChR KO (left), stage 2 (center), and stage 3 (right).

(B) Left, diagram of red and green set up; jRCaMP1b in retinal axons and GCaMP6f in SC. Right, example traces from each of the three “stages” shown above. Grey area in bottom indicates period depicted in montage at top.

(C) Correlation coefficient between presynaptic and postsynaptic activity (n=8 hemispheres nAChR KO, mean=0.149; n=9 hemispheres stage 2, mean=0.480; n=8 hemispheres stage 3, mean=0.308; nAChR significantly lower correlation, p=0.0106, Tukey’s multiple comparisons correction).

(D) Ratio of independent post-synaptic activity to independent pre-synaptic activity, where stage 2 and 3 are close to 1, but nAChR KO has significantly more post-synaptic activity relative to pre-synaptic (p=0.0018).

(E) Regression model used to examine the transfer of presynaptic (RGC) activity to postsynaptic (SC) activity. (i) Top panels show the presynaptic (β_1) coefficients that represent the contribution of nearby presynaptic activity to each postsynaptic pixel. The bottom panels display the contribution of surrounding postsynaptic activity (β_2 coefficients). (ii) Consistent with the independent presynaptic and postsynaptic activity in the nAChR KO mice, the regression model fit (R-squared) for stage 2 and stage 3 is high, and much stronger than in the nAChR KO mice. (iii) The spatial spread (weighted variance, see Methods) of the influence of the presynaptic RGC activity on postsynaptic activity (β_1 coefficient spread) is much larger in nAChR KO, but similar in stage 2 and stage 3. (iv) The strength of the

influence of presynaptic RGC activity on postsynaptic SC activity (β_1 coefficient amplitude) is similar in nAChR KO, stage 2 and stage 3 mice. See also Figure S1.
* = p<0.05, ** = p<0.01, *** = p<0.001.

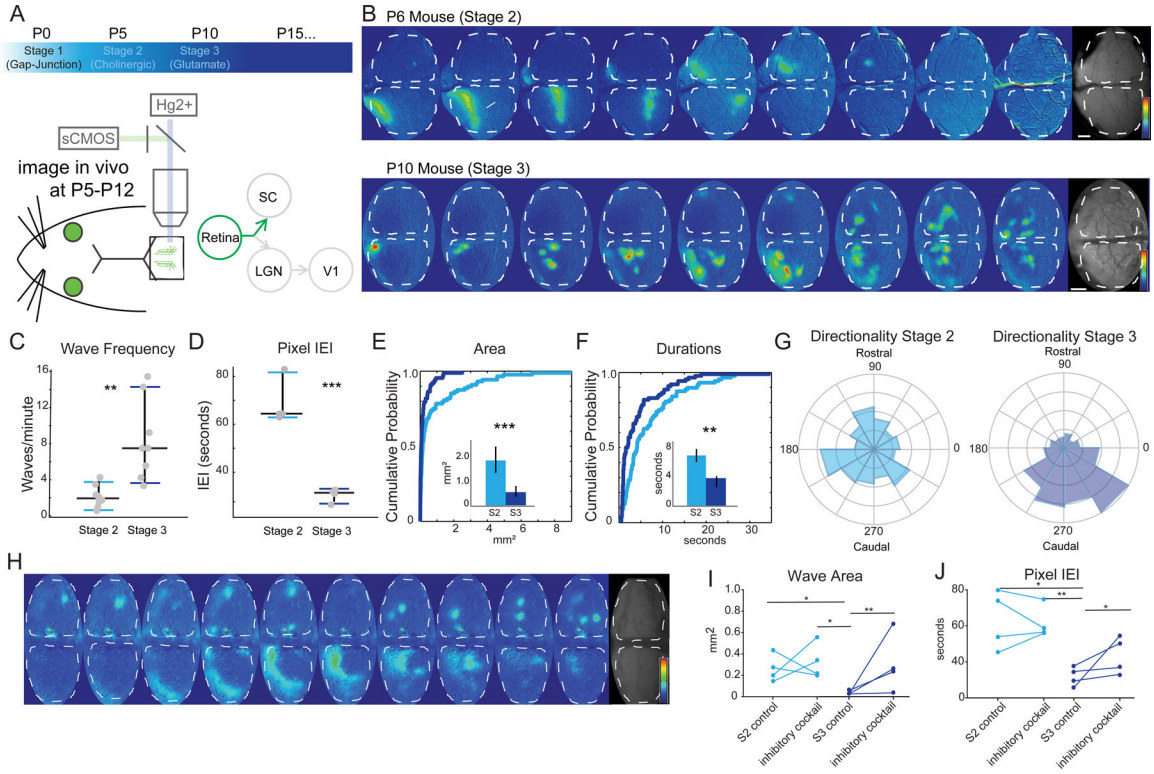

Figure 3: Stage 3 waves are very different than stage 2 waves

(A) Timeline of retinal waves and experimental set up for wide field imaging of spontaneous activity in the superior colliculus (SC).

(B) Montages of example stage 2 (P6, top) and stage 3 (P10, bottom) waves showing ΔF/F signal, each panel is two seconds apart, 16 seconds total (scale bars=200 μm) and (bottom) time course of activity over 5 minutes.

(C-D) Wave frequency properties of stage 2 and stage 3 waves (C), and inter-event interval (IEI) by pixel (D). Significant differences across a range of measures were apparent between stage 2 and stage 3 waves, n=7 mice for stage 2 and n=8 for stage 3. See also Figures S2 and S3.

(E-F) Cumulative probability distribution (by wave) and means (insets - by hemisphere) of wave activity. Stage 2 waves cover significantly greater area ($p = 0.0011$, K-S test) and are more long-lasting than stage 3 waves ($p = 0.0092$, K-S test). Light blue is stage 2, dark blue is stage 3.

(G) Stage 3 waves (right – P10-P12) are more likely to propagate in a rostral-to-caudal direction on the SC than stage 2 waves (left – P5-P8). Circular variance (CV) of all stage 2 waves 0.9354, CV of all stage 3 waves = 0.5110, $p=0.0137$ for t-test of individual CV.

(H) Montage of the effects of the inhibitory antagonist cocktail (500 mM TPMPA, 50 mM gabazine, and 5 uM strychnine) on stage 3 waves, which resemble stage 2 waves upon application of inhibitory antagonist cocktail to the retina. Saline control in the retina projection to the right hemisphere (top) and inhibitory antagonists in the retina projecting to the left hemisphere (bottom).

(I-J) Summary quantification of the effect of the inhibitory antagonist cocktail on stage 2 and stage 3 waves. Wave area (I) and inter-event (wave) interval (J) are unaltered by

application of the inhibitory antagonists during stage 2, but significantly affected during stage 3 (n=4 mice in each group; 4 control saline injected hemispheres and 4 with inhibitory cocktail). The effect of the inhibitory antagonists on stage 3 waves is to increase wave area and inter-event interval, resulting in waves that more closely resemble stage 2. See also Figure S2.

* = $p<0.05$, ** = $p<0.01$, *** = $p<0.001$.

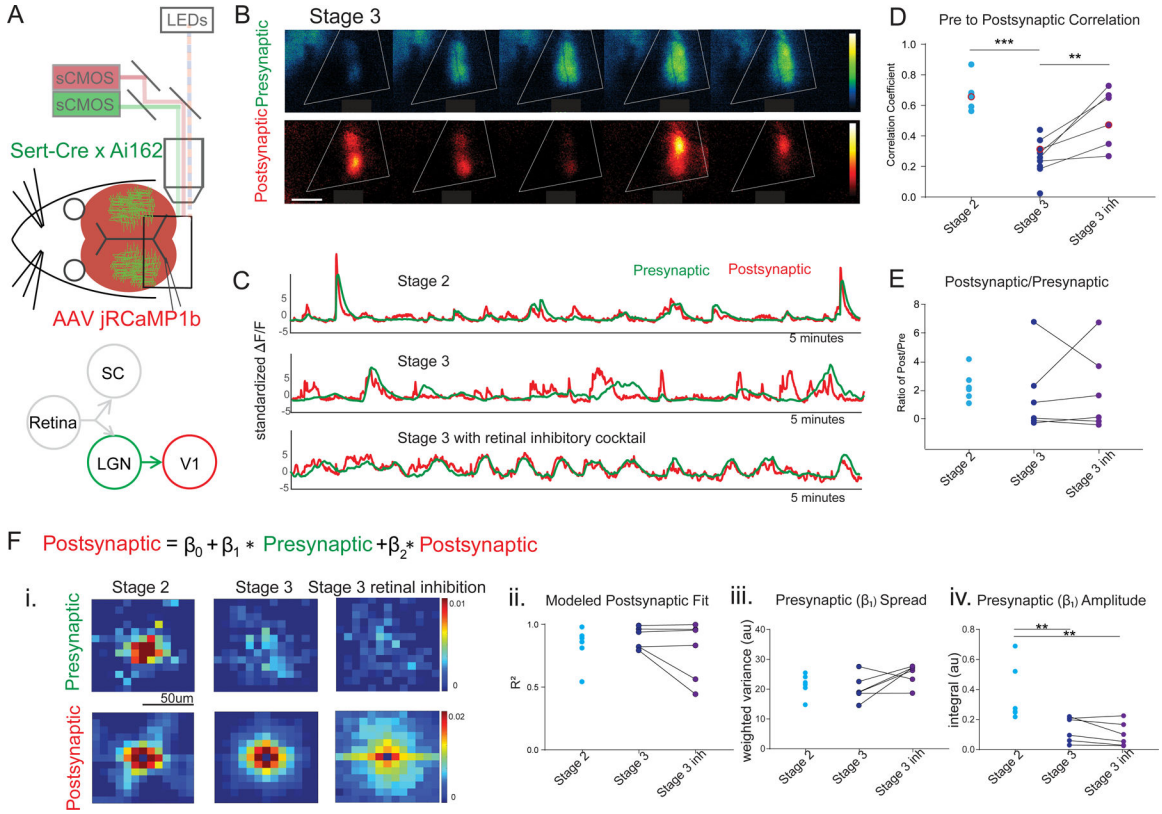

Figure 4: Transfer of wave activity between thalamus and cortex

(A). Experimental set up for simultaneous imaging of thalamic afferents and cortical activity using the same dual wavelength imaging protocol as described in Figure 1. Sert-Cre x Ai162 mice, which selectively express GCaMP6s in the thalamus, were used to image thalamic afferents in visual cortex. In addition, jRCaMP1b, expressed in the cortex pan-neuronally (see Methods), was used to image cortical activity.

(B). Example montage of stage 3 waves in which the presynaptic (green - GCaMP, thalamic afferents) and postsynaptic (red - RCaMP, cortex) activity show a mismatch. Scale bar 400um.

(C). Example traces of visual cortex wave activity in stage 2 (top), stage3 (middle), and stage 3 after blocking inhibition in the retina (bottom). Note mismatch in presynaptic (green - GCaMP, thalamic afferents) and postsynaptic (red - RCaMP, cortex) during stage 3.

(D). Correlation coefficient between presynaptic and postsynaptic activity during stage 2 and stage 3 waves before and after application of inhibitory antagonist cocktail to the retina. Presynaptic and postsynaptic activity are much less correlated in stage 3 than in stage 2, but altering stage 3 wave properties by application of inhibitory antagonists to the retina increases the correlation between presynaptic and postsynaptic neurons.

(E). The ratio of independent post-synaptic activity to independent pre-synaptic activity was not different across stage 2 and stage 3, with and without inhibitory antagonists.

(F). Regression model for presynaptic (thalamic axons) and postsynaptic (cortical neuron) activity as described in Figure 2. (i) Top panels show the presynaptic (β_1) coefficients that represent the contribution of nearby thalamic axon activity to each postsynaptic pixel. The bottom panels display the contribution of surrounding postsynaptic activity (β_2 coefficients).

(ii) Regression model fit (R^2) are comparable in all cases. (iii) The spatial spread (weighted variance, see Methods) of the influence of the presynaptic thalamic activity on postsynaptic activity (β_1 coefficient spread) is similar in stage 2 and stage 3. (iv) The strength of the influence of presynaptic thalamic activity on postsynaptic cortical activity (β_1 coefficient amplitude) is significantly higher in stage 2 than in stage 3 with or without inhibitory antagonists applied to the retina. See also Figure S4.

* = $p<0.05$, ** = $p<0.01$, *** = $p<0.001$.

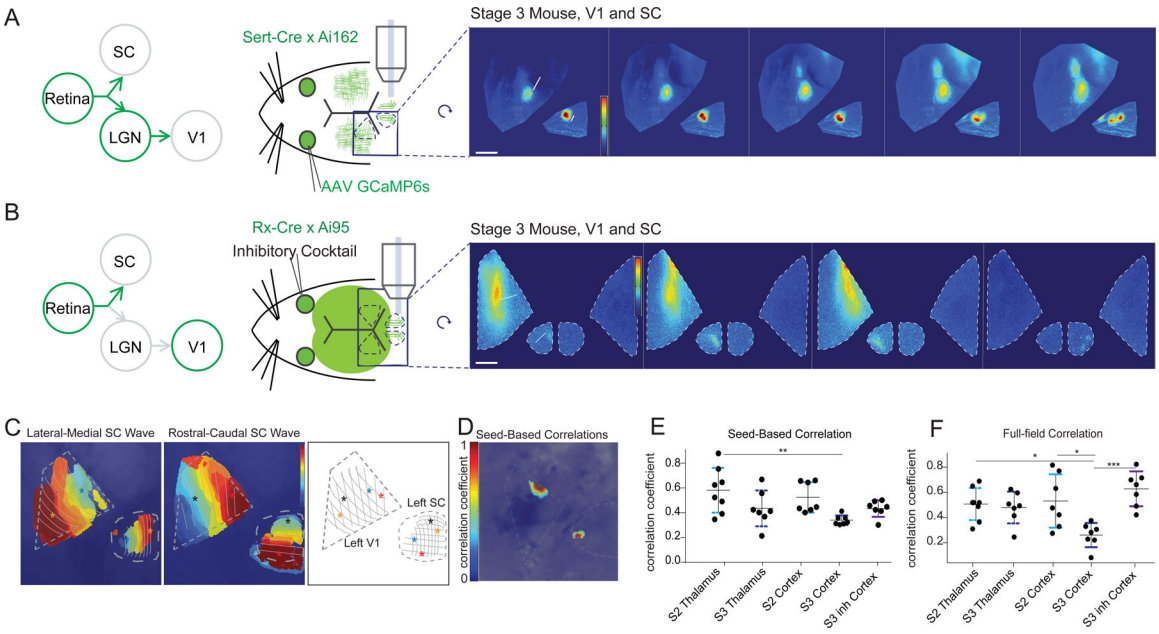

Figure 5: Stage 3 waves do not transfer to V1 as faithfully as Stage 2, or thalamus

(A). Experimental set up and montage example measuring retinal waves in the superior colliculus through AAV-mediated expression of GCaMP6s in RGCs and thalamic waves in the cortex through conditional expression of GCaMP6s in the thalamus (Sert-Cre x Ai162). Scale bar 300um.

(B). Experimental set up and montage example measuring retinal waves in the superior colliculus while simultaneously examining cortical waves through the conditional expression of GCaMP6s in both the retina and visual cortex (Rx-Cre x Ai162). Scale bar 400um. Left retina was treated with inhibitory cocktail, as described in Figure 3. Large, stage-2-like waves visible in both retinal axons of contralateral SC and contralateral V1. See also Figure S5.

(C) Two example waves in V1 and SC traveling in orthogonal directions. V1 retinotopic map is flipped and rotated approximately 90 degrees from SC map. Stars depict the position of the beginning and end of the waves.

(D). Example seed-based correlation where seed in lateral SC has a strong and localized correlation to its matched retinotopic position in rostral V1.

(E) Summary quantification of seed-based correlations between the retina and either thalamic or cortical activity during stage 2 and stage 3. The strength of seed-based correlations between RGC activity and dLGN (thalamus) activity was not significantly different in stage 3 compared to stage 2. However, the seed-based correlations between the retina and V1 during stage 3 was significantly smaller than the retina to the dLGN in stage 2. All statistics were corrected for multiple comparisons using Tukey's multiple comparisons correction.

(F) Summary quantification of full-field (imaged region in SC or V1) cross-correlations between the retina and either thalamic or cortical activity during stage 2 and stage 3. Stage 3 retinal waves had significantly lower correlation to V1 activity than in stage 2 and significantly lower correlation to dLGN in stage 2. Converting stage 3 waves to stage 2-like waves with the application of inhibitory antagonists to the retina significantly increased the

full-field correlation between RGCs and V1 activity so that it was indistinguishable from stage 2 correlations in the cortex or between the RGCs and the dLGN (thalamus). All statistics were corrected for multiple comparisons using Tukey's multiple comparisons correction.

* = $p<0.05$, ** = $p<0.01$, *** = $p<0.001$.

Table 1.

Three Spontaneous Wave Epochs

Stage 1	**Stage 2**	**Stage 3**
Age		
Late gestation	P0–P9	P10 eye opening
Excitatory drive		
Gap junction	acetylcholine	glutamate
In vitro wave propagation characteristics		
Large, brief waves (Syed et al., 2004) RRID: IMSR_JAX: 024105	large and slow waves with random trajectories	small, brief waves with repetitive trajectories

Key Resources Table

REAGENT or RESOURCE	SOURCE	IDENTIFIER
Bacterial and Virus Strains		
pAAV.Syn.NES-jRCaMP1b.WPRE.SV40	Dana et al., 2016	RRID:Addgene_100851
pAAV.Syn.GCaMP6f.WPRE.SV40	Chen et al., 2013	RRID:Addgene_100837
Chemicals, Peptides, and Recombinant Proteins		
(±)- epibatidine dihydrochloride hydrate	Sigma-Aldrich	E1145
NBQX	Tocris	Cat. No. 0190
APV	Tocris	Cat. No. 0106
Gabazine	Tocris	Cat. No. 1262
TPMPA	Sigma-Aldrich	T200
Strychnine	Sigma-Aldrich	S0532
Experimental Models: Organisms/Strains		
Mouse: Ai95(RCL-GCaMP6f)-D	Jackson Laboratories	RRID: IMSR_JAX:024105
Mouse: Ai162 (TIT2L-GC6s-ICL-tTA2)	Hongkui Zeng	RRID: IMSR_JAX:031562
Mouse: Rx-Cre	Swindell et al. (2006)	RRID:MGI:3665332
Mouse: Sert-Cre	Zhuang et al. (2005)	RRID:IMSR_JAX:014554
Mouse: En1-Cre	Jackson Laboratories	RRID:IMSR_JAX:007916
Software and Algorithms		
MATLAB	MathWorks	https://www.mathworks.com/products/matlab.html
ImageJ	NIH	https://imagej.nih.gov/ij/
Dual Wavelength Transfer Analysis	This Paper	https://github.com/agribizis/CrairLabCode